Published in final edited form as:

Cancer Res. 2019 March 15; 79(6): 1085–1097. doi:10.1158/0008-5472.CAN-18-0482.

Drak/STK17A drives neoplastic glial proliferation through modulation of MRLC signaling

Alexander S. Chen[1,*], **Joanna Wardwell-Ozgo**[1,*], **Nilang N. Shah**[1], **Deidre Wright**[1], **Christina L. Appin**[4,5], **Krishanthan Vigneswaran**[6], **Daniel J. Brat**[3,4,5], **Harley I. Kornblum**[7,8], **Renee D. Read**[1,2,3,9]

[1]Department of Pharmacology, Emory University School of Medicine, Atlanta, GA 30322

[2]Department of Hematology and Medical Oncology, Emory University School of Medicine, Atlanta, GA 30322

[3]Winship Cancer Center, Emory University School of Medicine, Atlanta, GA 30322

[4]Department of Pathology, Emory University School of Medicine, Atlanta, GA 30322

[5]Department of Pathology, Northwestern University Feinberg School of Medicine, Chicago, IL 60611

[6]Department of Neurosurgery, Emory University School of Medicine, Atlanta, GA 30322

[7]Department of Molecular and Medical Pharmacology, University of California – Los Angeles, Los Angeles, CA 90095

[8]Department of Psychiatry and Behavioral Sciences, and Semel Institute for Neuroscience and Human Behavior, University of California – Los Angeles, Los Angeles, CA 90095

Abstract

Glioblastoma (GBM) and lower grade gliomas (LGG) are the most common primary malignant brain tumors and are resistant to current therapies. Genomic analyses reveal that signature genetic lesions in GBM and LGG include copy gain and amplification of chromosome 7, amplification, mutation, and overexpression of receptor tyrosine kinases (RTK) such as EGFR, and activating mutations in components of the PI-3 kinase (PI3K) pathway. In *Drosophila melanogaster*, constitutive co-activation of RTK and PI3K signaling in glial progenitor cells recapitulates key features of human gliomas. Here we use this *Drosophila* glioma model to identify death-associated protein kinase (Drak), a cytoplasmic serine/threonine kinase orthologous to the human kinase STK17A, as a downstream effector of EGFR and PI3K signaling pathways. Drak was necessary for glial neoplasia, but not for normal glial proliferation and development, and Drak cooperated with EGFR to promote glial cell transformation. Drak phosphorylated Sqh, the *Drosophila* ortholog of MRLC (non-muscle myosin regulatory light chain), which was necessary for transformation. Moreover, Anillin, which is a binding partner of phosphorylated Sqh, was

[9)]corresponding author: renee.read@emory.edu, 404-727-5985.
[*)]co-first authors

Conflict of Interest: There are no conflicts of interest regarding this manuscript. Human tumor samples used in this manuscript were collected under informed consent as per an approved IRB protocols at University of California – Los Angeles and at Emory University.

upregulated in a Drak-dependent manner in mitotic cells and co-localized with phosphorylated Sqh in neoplastic cells undergoing mitosis and cytokinesis, consistent with their known roles in non-muscle myosin-dependent cytokinesis. These functional relationships were conserved in human GBM. Our results indicate that Drak/STK17A, its substrate Sqh/MRLC and the effector Anillin/ANLN regulate mitosis and cytokinesis in gliomas. This pathway may provide a new therapeutic target for gliomas.

INTRODUCTION

Glioblastomas (GBM), the most common primary malignant brain tumors, infiltrate the brain, grow rapidly, and are resistant to current therapies (1). Low grade gliomas (LGG), which are related infiltrative malignant neural neoplasms, have slower tumor growth rates, longer patient survival, and display more variable responses to therapeutics (2). To understand their genesis, these tumors have been subject to extensive genomic analyses, which show that signature genetic lesions in LGG and GBM include copy gain and amplification of chromosome 7, amplification, mutation, and/or overexpression of receptor tyrosine kinases (RTKs), such as EGFR, and activating mutations in components of the PI-3 kinase (PI3K) pathway (1, 3, 4). Nearly 60% of GBMs show focal EGFR copy gain or amplification, which are often accompanied by gain-of-function EGFR mutations (4). The most prevalent EGFR mutant variant in GBM is $EGFR^{VIII}$ (5), in which exon2-7 deletion confers constitutive kinase activity, which potently drives tumorigenesis (1, 6). The most frequent PI3K pathway mutation in gliomas is loss of PTEN lipid phosphatase (4), which results in unopposed PI3K signaling.

Recent mouse models demonstrate that co-activation of EGFR and PI3K pathways in glial cells or neuro-glial stems cells induces GBM-like tumors, although these tumors do not show the full range of GBM phenotypes (7-9). Furthermore, to date, pharmacologic inhibitors of EGFR and PI3K pathway components are ineffective in improving LGG and GBM outcomes (10). Genomic studies indicate that LGGs and GBMs have other genomic alterations (3-5); however, it is unknown how these changes contribute to gliomagenesis. Taken collectively, these data suggest that there are still undiscovered biological factors that drive tumorigenesis. Given the aggressive nature of these tumors, there is a pressing need to better understand their biology and to identify additional factors that could serve as new drug therapy targets.

To investigate the biology of malignant gliomas, we developed models in *Drosophila melanogaster* (11). *Drosophila* offers unique advantages for modeling gliomas: flies have orthologs for 70% of human genes, including most known gliomagenic genes (12); *Drosophila* neural and glial cell types are homologous to their human counterparts (13); and versatile genetic tools are available for *in vivo* cell-type specific gene manipulation including RNAi (14). Although *Drosophila* models cannot address all aspects of glioma biology, our model demonstrates that constitutive activation of EGFR and PI3K signaling in glial progenitor cells gives rise to malignant glial tumors that recapitulate key biological features of human gliomas (11).

To discover new pathways that contribute to EGFR-PI3K-mediated glioma, we performed a kinome-wide RNAi-based genetic screen in our EGFR-PI3K *Drosophila* GBM model (15). Kinases were screened because they are highly conserved in terms of protein function between *Drosophila* and mammalian systems. One of the top candidates from this screen was Drak (Death-associated protein kinase related) (15). Drak and its human ortholog, STK17A, are cytoplasmic serine/threonine kinases in the Drak subfamily of cytoplasmic death-associated protein (DAP) kinases, which regulate cytoskeletal dynamics, cytokinesis, and cell adhesion and mobility (16-18). In *Drosophila* development, Drak promotes epithelial morphogenesis, acting downstream of Rho-GTPase signaling to control the actin cytoskeleton through phosphorylation of Spaghetti Squash (Sqh) (18, 19). MRLC, the human Sqh ortholog, is a regulator of non-muscle myosin type II (NMII) motor proteins, and phosphorylated MRLC binds to NMII and stimulates NMII-dependent contractile activity to promote cytoskeletal re-organization, morphogenesis, and cytokinesis (20, 21). MRLC phosphorylation is dynamic and tightly regulated, which allows for precise temporal and spatial changes to the cytoskeleton (20). Like other Drak family kinases, STK17A, which is expressed in GBM (22), can directly phosphorylate purified MRLC protein *in vitro* (18, 23). However, little is known about the mechanisms by which Drak/STK17A promotes tumorigenesis.

Here we characterize genetic and functional requirements for Drak in EGFR- and PI3K-driven neoplastic glia. We report that Drak operates downstream and in concert with EGFR signaling to phosphorylate and activate Sqh to drive proliferation of neoplastic glia. Moreover, our data show that, in mitotic neoplastic glial cells undergoing cytokinesis, phosphorylated Sqh co-localizes with Anillin, a cytoskeletal protein and known Sqh binding partner (24), and that Anillin is required for proliferation of neoplastic glia. We show that these interactions are conserved in human gliomas. STK17A is overexpressed in primary human GBM and LGG tumors and patient-derived GBM cell cultures, and elevated STK17A expression correlates with elevated EGFR, MRLC phosphorylation, and ANLN (human Anillin ortholog) levels. STK17A activity is required for tumor cell proliferation and for elevated levels of MRLC phosphorylation and ANLN. Moreover, we found that STK17A, phosphorylated MRLC, and ANLN are all co-localized to the cleavage furrow in tumor cells undergoing cytokinesis. Taken together, our data suggests that Drak⁄STK17A potentiates EGFR signaling to drive activation of Sqh/MRLC, which in turn regulates mitosis in gliomas through effects on Anillin/ANLN.

MATERIALS AND METHODS

Drosophila Strains and culture conditions

Drosophila stocks were obtained from the Bloomington stock center and VDRC and the specific genotypes and stocks used are listed in the Supplemental Table 1 and Table 2. $Drak^{null}$($Drak^{del}$) was a gift of David Hipfner (18). $UAS\text{-}sqh^{D20D21}$ was a gift of Guang-Chao Chen (25). $UAS\text{-}dEGFR^{\lambda}$ was a gift of Trudi Schupbach. All stocks were cultured on standard corn meal molasses food at 25°C. Prior to publication, the $UAS\text{-}Drak^{dsRNA}$ stocks were validated by PCR amplification of the dsRNA element followed by sequence validation against the published sequence available at the VDRC. To create *UAS-Drak* and *UAS-*

Drak^{KD} (kinase dead) constructs, the RE12147 *Drak* cDNA was cloned into pUAS-T, site directed mutagenesis was used to convert Lys-66 to Ala, and the resulting DNA was injected into embryos and stocks for each construct were established and sequence verified. All genotypes were established by standard genetic crossing.

Immunohistochemistry

Larval brains were dissected with forceps, fixed in 4% paraformaldehyde, processed, stained, and imaged as previously described (11). The following antibodies were used: 8D12 mouse anti-Repo (1:10, Developmental Studies Hybridoma Bank), anti-phospho-S21-Sqh (1:500, gift of Robert Ward) (26), anti-Anillin (1:500, gift of Maria Giansanti) (27). Secondary antibodies were conjugated to Cy3 (1:150), Alexa-488, or Alexa-647 (1:100) (Jackson Laboratories). Brains were mounted on glass slides ventral side down in vectashield and whole mount imaged on a Zeiss LSM 700 confocal system. For experiments where protein levels were compared between genotypes, all samples were prepared, subjected to immunohistochemistry, imaged, and image processed in a parallel manner side by side. 6 or more brains were stained with each Ab combination, and representative images are shown for each result. All brain phenotypes shown were highly penetrant, with approximately 75-100% of animals showing the growth phenotypes described. Images were analyzed in Zeiss Zen Software and processed in Photoshop. Larval *Drosophila* brain hemisphere volumes were analyzed using Imaris software. Larval glial cells were counted manually in representative optical sections of age-matched brain hemispheres, matched for section plane. Statistical analyses were done using Prism.

Mammalian tissue culture

GBM39, shared by C. David James, was created from human GBMs serially xenografted. GBM157, GBM281, GBM301, and GBM309 gliomasphere cultures were derived at UCLA and maintained in culture as described (28). HNPCs were obtained from Lonza. U87 and U87-EGFR^{vIII} cells were gifts of Frank Furnari. Cell culture was performed as previously described (15). Lentiviral shRNAs were prepared and used as previously described on serum cultured cells and adherent serum-free cultured gliomasphere lines (15). WST-1 assays on shRNA-treated cells were performed as previously described (15). For immunofluorescence, U87-EGFR^{vIII} cells were plated on glass coverslips, fixed with 4% paraformaldehyde, and stained on the coverslips with anti-beta-tubulin (1:25, Developmental Studies Hybridoma Bank, AA4.3), anti-STK17A (1:1000, Sigma HPA037979), anti-ANLN (1:100, Sigma, HPA005680), anti-phospho-S19-MRLC (1:200, Abcam, ab2480; note this antibody detects S19 according to our sequence alignment and not S20), and/or DRAQ7 (Cell Signaling Technology, 1:200) to stain nuclear DNA and chromosomes.

Immunoblot Analysis

Cultured cells were collected and washed with 1xPBS and lysed in RIPA buffer containing protease and phosphatase inhibitors. Whole third instar larval brains were dissected were washed with 1xPBS and lysed in RIPA buffer containing protease and phosphatase inhibitors. The following antibodies were used for immunoblotting following the manufacturer's recommendations: anti-STK17A (1:1000, Sigma, HPA037979), anti-phospho-S19-MRLC (1:500, Cell Signaling 3671), anti-phospho-S19-MRLC (1:200,

Abcam, ab2480), anti-MRLC (1:500, Cell Signaling, 3672), anti-EGFR (1:5000, BD), anti-ANLN (1:500, Sigma, HPA005680) and anti-actin (1:200, Developmental Studies Hybridoma Bank, JLA20). Bands were quantified using ImageJ.

in silico Analysis

STK17A mRNA expression data was obtained from cBioportal (www.cbioportal.org) and exacted and analyzed using RStudio. All graphs and statistics were generated from this data using Prism (29, 30). The *in silico* analysis results shown here are based solely upon data generated by the TCGA Research Network (http://cancergenome.nih.gov) (2-4).

TMA processing

All human tumor specimens were collected from surgical specimens donated for research with written informed consent of patients and were collected and used according to recognized ethical guidelines (Declaration of Helsinki, CIOMS, Belmont Report, GCP, Nuremberg Code) in a protocol (IRB00045732) approved by the Institutional Review Board at Emory University. Paraffin embedded human brain tumor specimens and tumor tissue microarrays with matched control tissue were prepared and sectioned using the Winship Core Pathology Laboratory. Antigen retrieval and immunohistochemical staining was performed as specified by manufacturer's guidelines for each specific antibody (15). The following antibodies were used: anti-STK17A (1:1000, Sigma HPA037979), anti-ANLN (1:50, Sigma, HPA005680), anti-phospho-S19-MRLC (1:200, Abcam, ab2480), anti-EGFR (1:50, Cell Signaling Technology, 4267). Results were scored by neuropathologists according to standard clinical criteria on a scale of 1 and 2 (low staining), 3 or 4 (high staining, with 4 being more uniform), and images of immunoreactivity were taken on an Olympus DP72 CCD camera.

Statistical analyses

Comparisons between two groups were performed by Mann-Whitney U Test (nonparametric) for TCGA RNA-seq data analyses. Comparisons between of three or more groups, were performed by one-way ANOVA with multiple comparisons to experimental controls. Comparisons between two groups were done using either paired or unpaired parametric T-Tests. Fisher's exact test was used to analyze correlations in IHC data.

RESULTS

Drak is required for glial neoplasia in *Drosophila*

To understand GBM pathology, we developed a *Drosophila* GBM model. The model uses the glial-specific *repo-Gal4* transcriptional driver to co-overexpress constitutively active versions of dEGFR (dEGFR$^{\lambda}$) and dp110 (dp110^{CAAX}), the catalytic subunit of PI3K, that together drive malignant transformation of post-embryonic larval glia (11). The resulting glial tumors exhibit phenotypic and molecular characteristics similar to human GBM (11). To identify novel modifiers of EGFR-PI3K driven glial neoplasia, we used our *Drosophila* GBM model in a genetic screen, and identified Drak, which encodes the sole *Drosophila* ortholog of STK17A and STK17B serine/threonine kinases (15).

Glial-specific *Drak* RNAi reduced neoplastic glial proliferation and altered glial morphogenesis, with $Drak^{dsRNA\#1}$ yielding significantly reduced brain sizes and glial cell numbers compared to $dEGFR^{\lambda}$-$dp110^{CAAX}$ (Figure 1A-C, 1D-I). The transforming effects of EGFR-PI3K signaling were also reduced in *Drak* null mutants ($Drak^{null}$) (18) or by co-overexpression of kinase-dead Drak ($Drak^{KD}$): such mutants showed near wild-type brain sizes and reduced glial cell numbers compared to $dEGFR^{\lambda}$-$dp110^{CAAX}$ controls (Figure 1A-C, 1D-I), indicating that Drak catalytic activity is essential for proliferation of $dEGFR^{\lambda}$-$dp110^{CAAX}$-mutant glia.

Growth inhibition of neoplastic glia induced by *Drak* knockdown or loss-of-function was not due to nonspecific glial lethality: *Drak* is a nonessential gene and homozygous null mutants are viable and show normal brain morphology and glial development, and *Drak* RNAi in wild-type larval glia caused no obvious defects (15, 18) (Supplemental Figure S1A-B). Thus, while Drak is not required for normal glial proliferation and development, Drak kinase activity is essential for neoplastic glial proliferation.

Because reduced Drak function had a dramatic effect on $dEGFR^{\lambda}$-$dp110^{CAAX}$ mutant neoplastic glia, and because Drak functions downstream of EGFR in epithelia (19), we predicted that Drak may function downstream of EGFR in neoplastic glia. Overexpression of constitutively active $dEGFR^{\lambda}$ alone elicits hyperplasia in glia (11), which we found was suppressed by loss of *Drak* function (Supplemental Figure S1C-D), consistent with our prediction.

Previous studies show that, in developing epithelia, Drak acts downstream of EGFR and RhoGTPase (RhoA) signaling in parallel with Rho kinase (Rok) (18, 19). To investigate whether RhoGTPases are also required in neoplastic glia, we tested *RhoA* RNAi and dominant negative constructs in our GBM *Drosophila* model. We found that *RhoA* loss-of-function caused a significant reduction in $dEGFR^{\lambda}$-$dp110^{CAAX}$ mutant glial proliferation, but did not obviously affect wild-type glia proliferation (Figure 1A-C, 1D-I, Supplemental Table 1). Glial-specific inhibition of Rho family GTPases Cdc42 and RhoL and glial-specific *Rok* RNAi did not as strongly suppress neoplastic glial proliferation (15) (Supplemental Table 1). Thus, Drak may phosphorylate substrates to drive neoplastic glial proliferation downstream of RhoA GTPase signaling, independent of Rok. Together, our data demonstrate that Drak pathways are necessary for EGFR-PI3K-dependent glial neoplasia.

Drak cooperates with EGFR to promote glial transformation

Because Drak reduction suppressed glial neoplasia in the context of constitutive EGFR-PI3K and EGFR signaling, we tested whether Drak overexpression cooperates with constitutive EGFR signaling. We found that glial-specific Drak overexpression had no obvious effect on normal larval glia morphology or number compared to wild-type (Figure 2A-C). Glial-specific $dEGFR^{\lambda}$ overexpression induced a significant increase in glial cell numbers compared to wild-type controls (Figure 2A-D). (11). Co-overexpression of Drak and $dEGFR^{\lambda}$ increased glial cell numbers, and these glia lost their normal stellate shape and formed abnormal cellular aggregates that disrupted normal larval brain architecture, indicative of neoplastic transformation (Figure 2A-E). We previously showed that

overexpression of human EGFR^{vIII} (hEGFR^{vIII}), an oncogenic constitutively active mutant variant of EGFR found in GBM, cooperates with dp110^{CAAX} to drive neoplastic glial transformation, which was suppressed by Drak RNAi (15). Similar to dEGFR$^{\lambda}$, hEGFR^{vIII} overexpression caused glial hyperplasia (15), and Drak and hEGFR^{vIII} co-overexpression cooperated to drive increased proliferation and alterations in larval glial morphology consistent with neoplastic transformation (Supplemental Figure S2A-D). Thus, while Drak overexpression alone has little effect in glia, Drak co-overexpression augments the ability of constitutively active EGFR to promote tumorigenesis. Thus, Drak acts as a bona fide genetic modifier in that Drak loss or gain exerts the observed effects only in the context of other oncogenic mutations.

Drak acts downstream of oncogenic EGFR to phosphorylate Sqh

We next sought to understand the mechanism whereby Drak contributes to glial transformation. Given that Drak catalytic activity was essential for EGFR-PI3K glial neoplasia, we predicted that Spaghetti squash (Sqh), which is the *Drosophila* ortholog of human NMII regulatory light chain (MRLC) and only known Drak substrate (18), would be essential for EGFR-PI3K glial neoplasia. Prior studies have shown that DAP family kinases, including STK17A, the human ortholog of Drak, phosphorylate MRLC at serine and threonine residues (Thr-18 and Ser-19) (18, 21, 23). Similarly, Drak phosphorylates Sqh at the conserved serine residue (Ser-21 in Sqh is equivalent to Ser-19 in MRLC) (18, 21, 23). Phosphorylated Sqh binds to and stimulates the ATPase-dependent motor activity of Zipper, the sole NMII ortholog, which functions in cellular processes that require cytoskeletal contractility, such as cell migration, cytokinesis, and morphogenesis; all processes that play pivotal roles in tumorigenesis (21, 31, 32).

We found that, similar to *Drak* knockdown, glial-specific *sqh* knockdown significantly reduced glial cell numbers and rescued brain size in dEGFR$^{\lambda}$-dp110^{CAAX} mutants (Figure 3A-F), which suggests that Drak activates Sqh by phosphorylation in transformed glia. To test this hypothesis, we used a validated phospho-specific antibody to examine levels of Ser-21-phosphorylated Sqh (Sqh-S21-P) protein in dEGFR$^{\lambda}$-dp110^{CAAX} mutant glia in the presence or absence of Drak (26). dEGFR$^{\lambda}$-dp110^{CAAX} mutant glia showed increased Sqh-S21-P compared to wild-type glia, with mitotic cells showing cortical enrichment of Sqh-S21-P (Figure 3G), consistent with published observations regarding Sqh phosphorylation during cytokinesis (27). Drak RNAi reduced Sqh-S21-P levels (Figure 3G), indicative of loss of Sqh activation.

We next asked whether concurrent activation of EGFR and Drak signaling influences levels of activated Sqh. Consistent with Drak activity to phosphorylate Sqh, we observed increased levels of Sqh-S21-P in *dEGFR$^{\lambda}$;Drak^{OE}* glia compared to Drak-over expressing glia (Figure 3G). By western blot, we observed increased levels of Sqh-S21-P with *Drak^{OE};hEGFR^{vIII}* glia compared to hEGFR^{vIII}-overexpressing glia (Supplemental Figure S2E). These data are consistent with a model in which Drak increases the amount of activated, phosphorylated Sqh, which in turn supports EGFR-dependent tumorigenesis.

If Sqh phosphorylation promotes EGFR-dependent neoplasia, then overexpression of a phospho-mimetic version of Sqh should enhance oncogenic EGFR. A prior study engineered

a Sqh transgene with serine-21 and threonine-20 converted to aspartic acid (Sqh^{D20D21}) to mimic the phosphorylated state (33). As predicted, Sqh^{D20D21} and $dEGFR^{\lambda}$ co-overexpression increased numbers of small proliferative glia that disturbed normal larval brain architecture; these changes are indicative of enhanced hyperplasia and/or neoplastic transformation (Figure 4A-4E). Thus, Sqh is a functionally relevant Drak substrate in EGFR-PI3K-mediated glial neoplasia. Taken together, our data provide strong support for a model in which Drak cooperates with oncogenic EGFR signaling to create and sustain a pool of activated, phosphorylated Sqh necessary for glial cell transformation.

A Sqh binding partner, Anillin, is required for neoplastic growth.

Following determination that glial neoplasia in our GBM model requires Sqh, we next sought to determine which processes downstream of Sqh are essential in neoplastic glia. We used our *Drosophila* GBM model to test RNAi constructs against eight published Sqh binding partners (Supplemental Table 2). We found that glial-specific RNAi of *anillin*, which encodes a well-established Sqh binding partner and actin-binding scaffolding protein important for cytoskeletal reorganization during cytokinesis (24), significantly reduced $dEGFR^{\lambda}$-$dp110^{CAAX}$ mutant glia proliferation (Figure 5A-F). Thus, *anillin* RNAi in glial cells may interfere with cytokinesis, thereby inhibiting tumor cell proliferation.

To determine if Anillin is an effector of dEGFR-Drak-Sqh signaling, we tested glial-specific *anillin* knockdown in either $dEGFR^{\lambda};Drak^{OE}$ or $dEGFR^{\lambda};sqh^{D20D21}$ mutant glia, and observed a significant reduction in glial proliferation (Supplemental Figure S3A-G), indicating that Anillin operates downstream of dEGFR-Drak-Sqh signaling. In contrast, *anillin* knockdown in wild-type glia had no impact on glial cell proliferation compared to wild-type controls (Supplemental Figure S3A-G), showing a differential requirement for the Drak-Sqh-Anillin pathway in neoplastic glia, but not wild-type glia.

MRLC phosphorylation mediates cellular processes that require NMII-dependent cytoskeletal contractility, including mitosis and cytokinesis (21, 31, 32). Previous studies demonstrate that phosphorylated Sqh recruits Anillin to the cortex during mitosis, where it coordinates cytokinesis by linking actin and NMII/Zipper proteins in the contractile ring (24). During embryonic cellularization, Drak phosphorylation of Sqh is responsible for proper organization of contractile rings (34), most likely because Sqh phosphorylation was necessary for binding of Anillin to Zipper. To determine if Drak-dependent phosphorylation of Sqh is necessary for Anillin binding and/or localization in mitosis, we examined Anillin localization in relation to Sqh-S21-P in neoplastic $dEGFR^{\lambda}$-$dp110^{CAAX}$ glia. Consistent with their binding in mitotic glia, Sqh-S21-P and Anillin were co-localized and enriched at the cortex and cleavage furrow (observed in mitotic cells in all $dEGFR^{\lambda};dp110^{CAAX}$ brains imaged, n=8), and this enrichment was lost upon Drak depletion (in all $dEGFR^{\lambda};dp110^{CAAX};Drak^{dsRNA\#1}$ brains imaged, n=6) (Figure 5G). Moreover, overall Anillin levels were reduced by Drak depletion (Figure 5G). Thus, our data support a model wherein Drak-dependent phosphorylation of Sqh promotes Anillin binding to coordinately drive cytokinesis and proliferation in neoplastic glia.

STK17A expression correlates with EGFR status, phosphorylated MRLC levels, and ANLN expression in human tumors

To determine whether the Drak-Sqh-Anillin pathway operates in human GBM and/or LGGs, we examined expression and function of the human orthologs of Drak, STK17A and STK17B, and found that STK17A is overexpressed in GBMs (15). We next examined STK17A levels in a panel of patient-derived human GBM stem-cell containing gliomasphere (GSC) cultures. Compared to cultured normal human neural progenitor cells (HNPCs), $EGFR^{vIII}$-positive and EGFR-mutant GSC cultures express higher levels of STK17A and ANLN (Figure 6A). Moreover, in GSC cultures with high STK17A levels, we also saw a modest increase in Ser-19-phosphorylated MRLC (MRLC-S19-P) relative to HNPCs (Figure 6A). Thus, at the protein level, we observed that the relationships between EGFR, STK17A, ANLN (Anillin), and MRLC phosphorylation in GBM cells recapitulate our observations from *Drosophila*.

To further explore pathway conservation, we examined STK17A function and localization in serum-cultured GBM cell lines and GSC lines using RNAi and immunofluorescence. Consistent with prior reports (22), we found that, in serum cultured lines, STK17A is required for proliferation, with STK17A knockdown inducing slower proliferation, apoptosis, reduced MRLC-S19-P levels, and altered cell shape and adhesion (Figure 6B, Supplemental Figure S4A-B), which is consistent with alterations in MRLC regulation (35-37). We examined the effects of STK17A loss in GSCs treated with or without ZVAD to control for the effects of apoptosis, and we found that STK17A knockdown caused GSC adhesion defects, slower proliferation, apoptosis, and reduced levels of MRLC-S19-P and ANLN levels relative to control GSCs (Figure 6C-D, Supplemental Figure S4C-D). We also observed that total MRLC levels were reduced upon STK17A knockdown, suggesting that phosphorylation may regulate total MRLC protein in GBM cells. This is consistent with published studies showing MRLC levels are regulated by proteosomal turn-over (38). Furthermore, we examined STK17A localization in $EGFR^{vIII}$-positive GBM cells and observed that STK17A protein, in conjunction with MRLC-S19-P and ANLN, was upregulated in mitotic cells and localized to the cleavage furrow in tumor cells undergoing cytokinesis (Figure 6E-F). Thus, STK17A expression is required to promote MRLC phosphorylation and ANLN upregulation in GBM cells to coordinately regulate cytokinesis and proliferation.

We used immunohistochemistry to examine protein expression of STK17A, EGFR, MRLC-S19-P, and ANLN in a collection of graded human tumor specimens. In LGG tissue microarrays (TMA), specimens with high STK17A expression showed a statistically significant correlation with high EGFR, MRLC-S19-P, and ANLN expression (Figure 7A). In GBM TMAs, we observed high expression of EGFR, STK17A, MRLC-S19-P, and ANLN in the majority of specimens (Figure 7B). However, we observed some GBM specimens with high STK17A but low MRLC-S19-P expression (Figure 7B): in these surgical GBM specimens, it is possible that the MRLC-S19-P phospho-epitope was not properly fixed and preserved. Thus, in human tumors, elevated STK17A levels co-occur with elevated EGFR, MRLC-S19-P, and ANLN levels, which recapitulates the relationship we observed between EGFR, Drak, Sqh, and Anillin in *Drosophila*.

We used cBioportal to process genomic data catalogued by The Cancer Genome Atlas (TCGA) to assess prevalence of *STK17A* mRNA expression and copy gain alterations and to examine relationships between STK17A alterations and well-characterized genetic lesions in gliomas (2-4, 29, 30). Well-characterized lesions include full or partial amplification of chromosome 7, which includes regions encoding both *EGFR* and *STK17A* (39), and focal *EGFR* amplification and mutation. In TCGA cohorts of LGGs and GBMs, *STK17A* mRNA expression was significantly correlated with copy number gain in 13p on chromosome 7 (7p13) (Figure7C-D). To understand whether *STK17A* mRNA overexpression is specific or is passively driven by copy gain, we examined mRNA expression of neighboring genes on chromosome 7. We found that genes in close proximity to *STK17A* (i.e. *NACAD)* showed no statistically significant difference in mRNA expression between LGG specimens with chromosome 7 copy gain compared to LGG specimens with no observable copy number alterations in the same region of chromosome 7 (Figure 7E), indicating that *STK17A* mRNA expression may be selectively upregulated. Thus, increased *STK17A* expression may have a specific role in glioma pathology.

To further assess whether STK17A is a driver of gliomagenesis, we used cBioportal to examine *STK17A* mRNA expression relative to IDH1 status in LGG patients. *IDH1* mutation is a common genetic alteration in LGG, and patients who harbor *IDH1* mutations have a better prognosis than those with wild-type *IDH1* (40-42). LGG patients with wild-type *IDH1* have more aggressive tumors that behave much like primary GBMs (2, 40). Furthermore, wild-type *IDH1*, not mutant *IDH1*, is typically found in gliomas with chromosome 7 alterations (2, 40). In LGG, we found elevated *STK17A* mRNA expression in tumors with wild-type *IDH1* compared to tumors with mutant *IDH1* (Figure 7F). In *IDH1* mutant LGGs, there was not a statistically significant difference between *STK17A* mRNA expression between tumors with or without chromosome 7 gain (Figure 7G), suggesting that STK17A levels are not as relevant to progression in *IDH1* mutant tumors. Our observations are consistent with a previous study showing *STK17A* mRNA overexpression in LGGs is correlated with disease severity and worse prognosis (22).

To investigate associations between *STK17A* expression and patient survival, we analyzed cBioportal TCGA data to find that LGG and GBM patients with at least two-fold *STK17A* copy gain showed worse overall survival compared to patients with no *STK17A* copy gain (Supplemental Figure S5A-B). Thus, LGG and GBM patients with STK17A copy gain have a worse overall prognosis.

Together, our results suggest that elevated STK17A expression drives MRLC and ANLN dependent cytoskeletal changes during mitosis and cytokinesis to facilitate disease progression (Figure 7H), validating our identification of the STK17A ortholog Drak as a driver of tumorigenesis in our *Drosophila* GBM model.

DISCUSSION

Though EGFR and PI3K pathways play important roles in glioma progression and maintenance, effective therapies targeting these pathways remain elusive (10). We developed a *Drosophila melanogaster* GBM model based on co-activation of EGFR and PI3K in glia in

order to gain insight into genetic and cellular mechanisms underlying gliomas (11, 15). Using our system, we identified a pathway through which the cytoplasmic serine/threonine kinase Drak specifically drives neoplastic proliferation. Consistent with published results (22), we show that the orthologous kinase STK17A drives proliferation human GBM cells, through a conserved pathway that regulates cytokinesis.

During *Drosophila* development, Drak acts downstream of EGFR and Rho-GTPase signaling to regulate epithelial tissue morphogenesis through Sqh phosphorylation (18, 19). Activated Sqh, like human MRLC, modulates cytoskeletal reorganization in cellular processes such as cytokinesis (32, 33, 43), which is fundamental to cancer progression (44). Drak harbors latent oncogenic activity, as it can cooperate with constitutively active EGFR to stimulate glial transformation. Similarly, in human LGG and GBM, STK17A is frequently subject to copy gain and overexpression in association with EGFR and chromosome 7 alterations. We show that, in *Drosophila* and human tumor cells, Sqh/MRLC is a key mediator of Drak/STK17A: Sqh/MRLC is phosphorylated at equivalent conserved sites in EGFR-PI3K mutant tumor cells in a Drak/STK17A-dependent manner, and is necessary for neoplastic growth. Thus, Sqh/MRLC is a functionally relevant and evolutionarily conserved substrate of Drak/STK17A in the context of EGFR-PI3K-driven glial tumorigenesis. This corroborates studies that have shown MRLC hyper-phosphorylation occurs in GBM tumors and that targeted inhibition of MRLC activity inhibits GBM growth and invasion (35-37, 45, 46). Together, our results establish STK17A as a disease-relevant MRLC kinase in gliomas.

MRLC phosphorylation regulates many cellular processes that require NMII-dependent contractility (21, 31, 32). To distinguish which of these processes are most relevant to Drak/STK17A function, we used a genetic approach and found that, among known Sqh binding partners, Anillin is essential in neoplastic glia. Anillin is a scaffolding protein that acts downstream of RhoGTPase to organize the cytoskeleton and contractile ring in cytokinesis (24, 47-50). As part of this functionality, Anillin binds to Zipper (NMII) when Sqh is phosphorylated and activated (24). Drak-dependent activation of Sqh promotes Anillin binding to Zipper and organization into contractile rings during cytokinesis (32, 34). We observed that phosphorylated Sqh and Anillin co-localize in a Drak-dependent manner at the cleavage furrow in EGFR-PI3K mutant glia undergoing cytokinesis. Similarly, we observed that elevated levels of phosphorylated MRLC, ANLN, and STK17A co-occur in human gliomas, and that these proteins co-localize at the cleavage furrow in EGFR-mutant GBM cells undergoing cytokinesis. Our results suggest that the primary role of Drak/STK17A in neoplastic glia is to promote cytokinesis to drive proliferation.

Two other MRLC kinases, MLCK and ROCK, and two different NMII isoforms, including NMIIA and NMIIB, regulate GBM cell migration (35-37, 45, 46). Previous studies also show that STK17A promotes GBM cell migration *in vitro* (22). Therefore, we did not study STK17A function in tumor cell invasion; instead, given the effects of Drak loss, we focused on Drak/STK17A function in GBM proliferation and cytokinesis. While regulation of cytokinesis in glioma cells is not well understood, our results imply that cytokinesis in glioma cells is differentially regulated relative to normal developing glia or neural stem cells. In other tumor cell types, cytokinesis is preferentially controlled by NMIIC, which is also expressed in GBM cells (45), and may therefore mediate STK17A function. Further

work is needed to determine mechanisms of Drak/STK17A dependent regulation of cytokinesis, and whether defective cytokinesis actively provokes growth arrest and apoptosis in GBM cells.

While Drak overexpression alone causes no phenotype, Drak overexpression intensified the proliferative output of EGFR and PI3K signaling pathways through Sqh. Given that Drak modifies glial EGFR-PI3K-driven neoplasia but does not affect normal glial development, Drak and STK17A may require other signaling outputs downstream of EGFR or PI3K to drive proliferation. This is consistent with known requirements for RTK and PI3K activity in cytokinesis and other NMII-dependent processes (32). For example, previous reports indicate that increased phosphorylation of NMII occurs in GBM cells in response to EGFR signaling (37). Thus, perhaps EGFR-dependent differential phosphorylation and activation of NMII underlies the mechanism by which Drak-Sqh and EGFR cooperate to drive tumorigenesis, and the lack of NMII phosphorylation underlies the inability of Drak to promote glial proliferation when overexpressed alone. Further studies are required to explore mechanisms by which Drak/STK17A cooperates with EGFR activation to promote tumorigenesis.

In summary, our data validate use of invertebrate model organisms as a means to elucidate new aspects of glioma biology. Our research reveals that Drak/STK17A dependency may provide a molecular vulnerability and therapeutically relevant target for GBM and LGG.

Supplementary Material

Refer to Web version on PubMed Central for supplementary material.

Acknowledgements

We thank Tim Fenton, Clay Coston Rowe, Colleen Mosley, and Hye Rim Kim for technical assistance, and Ken Moberg for critical reading of the manuscript.

Funding: This work was supported by grants from the NIH/NINDS (NS065974, NS100967), the Southeastern Brain Tumor Foundation, and Emory University Research Committee to R. D. Read, and a K12-IRACDA career development award from the NIH/NIGMS (GM000680) to J. Wardwell-Ozgo. This work was also supported by grant NS100967 from NIH/NINDS to R.D. Read.

References:

1. Dunn GP, Rinne ML, Wykosky J, Genovese G, Quayle SN, Dunn IF, Agarwalla PK, Chheda MG, Campos B, Wang A, Brennan C, Ligon KL, Furnari F, Cavenee WK, Depinho RA, Chin L, Hahn WC. Emerging insights into the molecular and cellular basis of glioblastoma. Genes Dev. 2012;26(8):756–84. Epub 2012/04/18. doi: 10.1101/gad.187922.112. PubMed PMID: 22508724; PMCID: PMC3337451. [PubMed: 22508724]
2. Cancer Genome Atlas Research N, Brat DJ, Verhaak RG, Aldape KD, Yung WK, Salama SR, Cooper LA, Rheinbay E, Miller CR, Vitucci M, Morozova O, Robertson AG, Noushmehr H, Laird PW, Cherniack AD, Akbani R, Huse JT, Ciriello G, Poisson LM, Barnholtz-Sloan JS, Berger MS, Brennan C, Colen RR, Colman H, Flanders AE, Giannini C, Grifford M, Iavarone A, Jain R, Joseph I, Kim J, Kasaian K, Mikkelsen T, Murray BA, O'Neill BP, Pachter L, Parsons DW, Sougnez C, Sulman EP, Vandenberg SR, Van Meir EG, von Deimling A, Zhang H, Crain D, Lau K, Mallery D, Morris S, Paulauskis J, Penny R, Shelton T, Sherman M, Yena P, Black A, Bowen J, Dicostanzo K, Gastier-Foster J, Leraas KM, Lichtenberg TM, Pierson CR, Ramirez NC, Taylor C, Weaver S, Wise L, Zmuda E, Davidsen T, Demchok JA, Eley G, Ferguson ML, Hutter CM, Mills Shaw KR,

Ozenberger BA, Sheth M, Sofia HJ, Tarnuzzer R, Wang Z, Yang L, Zenklusen JC, Ayala B, Baboud J, Chudamani S, Jensen MA, Liu J, Pihl T, Raman R, Wan Y, Wu Y, Ally A, Auman JT, Balasundaram M, Balu S, Baylin SB, Beroukhim R, Bootwalla MS, Bowlby R, Bristow CA, Brooks D, Butterfield Y, Carlsen R, Carter S, Chin L, Chu A, Chuah E, Cibulskis K, Clarke A, Coetzee SG, Dhalla N, Fennell T, Fisher S, Gabriel S, Getz G, Gibbs R, Guin R, Hadjipanayis A, Hayes DN, Hinoue T, Hoadley K, Holt RA, Hoyle AP, Jefferys SR, Jones S, Jones CD, Kucherlapati R, Lai PH, Lander E, Lee S, Lichtenstein L, Ma Y, Maglinte DT, Mahadeshwar HS, Marra MA, Mayo M, Meng S, Meyerson ML, Mieczkowski PA, Moore RA, Mose LE, Mungall AJ, Pantazi A, Parfenov M, Park PJ, Parker JS, Perou CM, Protopopov A, Ren X, Roach J, Sabedot TS, Schein J, Schumacher SE, Seidman JG, Seth S, Shen H, Simons JV, Sipahimalani P, Soloway MG, Song X, Sun H, Tabak B, Tam A, Tan D, Tang J, Thiessen N, Triche T Jr., Van Den Berg DJ, Veluvolu U, Waring S, Weisenberger DJ, Wilkerson MD, Wong T, Wu J, Xi L, Xu AW, Yang L, Zack TI, Zhang J, Aksoy BA, Arachchi H, Benz C, Bernard B, Carlin D, Cho J, DiCara D, Frazer S, Fuller GN, Gao J, Gehlenborg N, Haussler D, Heiman DI, Iype L, Jacobsen A, Ju Z, Katzman S, Kim H, Knijnenburg T, Kreisberg RB, Lawrence MS, Lee W, Leinonen K, Lin P, Ling S, Liu W, Liu Y, Liu Y, Lu Y, Mills G, Ng S, Noble MS, Paull E, Rao A, Reynolds S, Saksena G, Sanborn Z, Sander C, Schultz N, Senbabaoglu Y, Shen R, Shmulevich I, Sinha R, Stuart J, Sumer SO, Sun Y, Tasman N, Taylor BS, Voet D, Weinhold N, Weinstein JN, Yang D, Yoshihara K, Zheng S, Zhang W, Zou L, Abel T, Sadeghi S, Cohen ML, Eschbacher J, Hattab EM, Raghunathan A, Schniederjan MJ, Aziz D, Barnett G, Barrett W, Bigner DD, Boice L, Brewer C, Calatozzolo C, Campos B, Carlotti CG Jr., Chan TA, Cuppini L, Curley E, Cuzzubbo S, Devine K, DiMeco F, Duell R, Elder JB, Fehrenbach A, Finocchiaro G, Friedman W, Fulop J, Gardner J, Hermes B, Herold-Mende C, Jungk C, Kendler A, Lehman NL, Lipp E, Liu O, Mandt R, McGraw M, McLendon R, McPherson C, Neder L, Nguyen P, Noss A, Nunziata R, Ostrom QT, Palmer C, Perin A, Pollo B, Potapov A, Potapova O, Rathmell WK, Rotin D, Scarpace L, Schilero C, Senecal K, Shimmel K, Shurkhay V, Sifri S, Singh R, Sloan AE, Smolenski K, Staugaitis SM, Steele R, Thorne L, Tirapelli DP, Unterberg A, Vallurupalli M, Wang Y, Warnick R, Williams F, Wolinsky Y, Bell S, Rosenberg M, Stewart C, Huang F, Grimsby JL, Radenbaugh AJ, Zhang J. Comprehensive, Integrative Genomic Analysis of Diffuse Lower-Grade Gliomas. N Engl J Med. 2015;372(26):2481–98. doi: 10.1056/NEJMoa1402121. PubMed PMID: 26061751; PMCID: PMC4530011. [PubMed: 26061751]

3. Comprehensive genomic characterization defines human glioblastoma genes and core pathways. Nature. 2008;455(7216):1061–8. Epub 2008/09/06. doi: 10.1038/nature07385. PubMed PMID: 18772890; PMCID: PMC2671642. [PubMed: 18772890]
4. Brennan CW, Verhaak RGW, McKenna A, Campos B, Noushmehr H, Salama SR, Siyuan Zheng S, Chakravarty D, Sanborn JZ, Berman SH, Beroukhim R, Bernard B, Wu C-J, Genovese G, Shmulevich I, Barnholtz-Sloan J, Zou L, Vegesna R, Shukla SA, Ciriello G, Yung WK, Zhang W, Sougnez C, Mikkelsen T, Aldape K, Bigner DD, Van Meir EG, Prados M, Sloan A, Black KL, Eschbacher J, Finocchiaro G, Friedman W, Andrews DW, Guha A, Iacocca M, ONeill BP, Foltz G, Myers J, Weisenberger DJ, Penny R, Kucherlapati R, Perou CM, Hayes DN, Gibbs R, Marra M, Mills GB, Lander E, Spellman P, Wilson R, Sander C, Weinstein J, Meyerson M, Gabriel S, Laird PW, Haussler D, Getz G, Chin L, Network TR. The Somatic Genomic Landscape of Glioblastoma. Cell. 2013;155(2): 462–77. [PubMed: 24120142]
5. Verhaak RG, Hoadley KA, Purdom E, Wang V, Qi Y, Wilkerson MD, Miller CR, Ding L, Golub T, Mesirov JP, Alexe G, Lawrence M, O'Kelly M, Tamayo P, Weir BA, Gabriel S, Winckler W, Gupta S, Jakkula L, Feiler HS, Hodgson JG, James CD, Sarkaria JN, Brennan C, Kahn A, Spellman PT, Wilson RK, Speed TP, Gray JW, Meyerson M, Getz G, Perou CM, Hayes DN. Integrated genomic analysis identifies clinically relevant subtypes of glioblastoma characterized by abnormalities in PDGFRA, IDH1, EGFR, and NF1. Cancer Cell. 2010;17(1):98–110. Epub 2010/02/05. doi: S1535-6108(09)00432-2 [pii] 10.1016/j.ccr.2009.12.020. PubMed PMID: 20129251. [PubMed: 20129251]
6. Nishikawa R, Ji XD, Harmon RC, Lazar CS, Gill GN, Cavenee WK, Huang HJ. A mutant epidermal growth factor receptor common in human glioma confers enhanced tumorigenicity. Proc Natl Acad Sci U S A. 1994;91(16):7727–31. Epub 1994/08/02. PubMed PMID: 8052651. [PubMed: 8052651]
7. Bachoo RM, Maher EA, Ligon KL, Sharpless NE, Chan SS, You MJ, Tang Y, DeFrances J, Stover E, Weissleder R, Rowitch DH, Louis DN, DePinho RA. Epidermal growth factor receptor and Ink4a/Arf: convergent mechanisms governing terminal differentiation and transformation along the

neural stem cell to astrocyte axis. Cancer Cell. 2002;1(3):269–77. PubMed PMID: 12086863. [PubMed: 12086863]

8. Zhu H, Acquaviva J, Ramachandran P, Boskovitz A, Woolfenden S, Pfannl R, Bronson RT, Chen JW, Weissleder R, Housman DE, Charest A. Oncogenic EGFR signaling cooperates with loss of tumor suppressor gene functions in gliomagenesis. Proc Natl Acad Sci U S A. 2009;106(8):2712–6. doi: 10.1073/pnas.0813314106. PubMedPMID:19196966;PMCID:2650331. [PubMed: 19196966]
9. Holland EC, Hively WP, DePinho RA, Varmus HE. A constitutively active epidermal growth factor receptor cooperates with disruption of G1 cell-cycle arrest pathways to induce glioma-like lesions in mice. Genes Dev. 1998;12(23):3675–85. PubMed PMID: 9851974. [PubMed: 9851974]
10. Cloughesy TF, Cavenee WK, Mischel PS. Glioblastoma: from molecular pathology to targeted treatment. Annual review of pathology. 2014;9:1–25. doi: 10.1146/annurev-pathol-011110-130324. PubMed PMID: 23937436.
11. Read RD, Cavenee WK, Furnari FB, Thomas JB. A drosophila model for EGFR-Ras and PI3K-dependent human glioma. PLoS Genet. 2009;5(2):e1000374. Epub 2009/02/14. doi: 10.1371/journal.pgen.1000374. PubMed PMID: 19214224. [PubMed: 19214224]
12. Reiter LT, Bier E. Using Drosophila melanogaster to uncover human disease gene function and potential drug target proteins. Expert Opin Ther Targets. 2002;6(3):387–99. PubMed PMID: 12223075. [PubMed: 12223075]
13. Freeman MR, Doherty J. Glial cell biology in Drosophila and vertebrates. Trends Neurosci. 2006;29(2):82–90. Epub 2005/12/27. doi: S0166-2236(05)00307-3 [pii] 10.1016/j.tins.2005.12.002. PubMed PMID: 16377000. [PubMed: 16377000]
14. Gonzalez C Drosophila melanogaster: a model and a tool to investigate malignancy and identify new therapeutics. Nat Rev Cancer. 2013;13(3):172–83. Epub 2013/02/08. doi: 10.1038/nrc3461. PubMed PMID: 23388617. [PubMed: 23388617]
15. Read RD, Fenton TR, Gomez GG, Wykosky J, Vandenberg SR, Babic I, Iwanami A, Yang H, Cavenee WK, Mischel PS, Furnari FB, Thomas JB. A kinome-wide RNAi screen in Drosophila Glia reveals that the RIO kinases mediate cell proliferation and survival through TORC2-Akt signaling in glioblastoma. PLoS Genet. 2013;9(2):e1003253. Epub 2013/03/06. doi: 10.1371/journal.pgen.1003253PGENETICS-D-12-01408 [pii]. PubMed PMID: 23459592. [PubMed: 23459592]
16. Lin Y, Hupp TR, Stevens C. Death-associated protein kinase (DAPK) and signal transduction: additional roles beyond cell death. The FEBS journal. 2010;277(1):48–57. Epub 2009/11/03. doi: 10.1111/j.1742-4658.2009.07411.x. PubMed PMID: 19878313. [PubMed: 19878313]
17. Bialik S, Kimchi A. The death-associated protein kinases: structure, function, and beyond. Annu Rev Biochem. 2006;75:189–210. Epub 2006/06/08. doi: 10.1146/annurev.biochem.75.103004.142615. PubMed PMID: 16756490. [PubMed: 16756490]
18. Neubueser D, Hipfner DR. Overlapping roles of Drosophila Drak and Rok kinases in epithelial tissue morphogenesis. Mol Biol Cell. 2010;21(16):2869–79. Epub 2010/06/25. doi: E10-04-0328 [pii] 10.1091/mbc.E10-04-0328. PubMed PMID: 20573980. [PubMed: 20573980]
19. Robertson F, Pinal N, Fichelson P, Pichaud F. Atonal and EGFR signalling orchestrate rok- and Drak-dependent adherens junction remodelling during ommatidia morphogenesis. Development. 2012;139(18):3432–41. Epub 2012/08/10. doi: dev.080762 [pii] 10.1242/dev.080762. PubMed PMID: 22874916. [PubMed: 22874916]
20. Vicente-Manzanares M, Ma X, Adelstein RS, Horwitz AR. Non-muscle myosin II takes centre stage in cell adhesion and migration. Nat Rev Mol Cell Biol. 2009;10(11):778–90. doi: 10.1038/nrm2786. PubMed PMID: 19851336; PMCID: 2834236. [PubMed: 19851336]
21. Heissler SM, Manstein DJ. Nonmuscle myosin-2: mix and match. Cell Mol Life Sci. 2013;70(1):1–21. Epub 2012/05/09. doi: 10.1007/s00018-012-1002-9. PubMed PMID: 22565821; PMCID: PMC3535348. [PubMed: 22565821]
22. Mao P, Hever-Jardine MP, Rahme GJ, Yang E, Tam J, Kodali A, Biswal B, Fadul CE, Gaur A, Israel MA, Spinella MJ. Serine/threonine kinase 17A is a novel candidate for therapeutic targeting in glioblastoma. PLoS One. 2013;8(11):e81803. Epub 2013/12/07. doi: 10.1371/journal.pone.0081803PONE-D-13-25674 [pii]. PubMed PMID: 24312360. [PubMed: 24312360]

23. Sanjo H, Kawai T, Akira S. DRAKs, novel serine/threonine kinases related to death-associated protein kinase that trigger apoptosis. J Biol Chem. 1998;273(44):29066–71. Epub 1998/10/24. PubMed PMID: 9786912. [PubMed: 9786912]
24. Straight AF, Field CM, Mitchison TJ. Anillin binds nonmuscle myosin II and regulates the contractile ring. Mol Biol Cell. 2005;16(1):193–201. Epub 2004/10/22. doi: 10.1091/mbc.E04-08-0758. PubMed PMID: 15496454; PMCID: PMC539163. [PubMed: 15496454]
25. Tang HW, Wang YB, Wang SL, Wu MH, Lin SY, Chen GC. Atg1-mediated myosin II activation regulates autophagosome formation during starvation-induced autophagy. EMBO J. 2011;30(4):636–51. Epub 2010/12/21. doi: 10.1038/emboj.2010.338. PubMed PMID: 21169990; PMCID: PMC3041946. [PubMed: 21169990]
26. Zhang L, Ward REt. Distinct tissue distributions and subcellular localizations of differently phosphorylated forms of the myosin regulatory light chain in Drosophila. Gene Expr Patterns. 2011;11(1-2):93–104. Epub 2010/10/06. doi: 10.1016/j.gep.2010.09.008. PubMed PMID: 20920606; PMCID: PMC3025304. [PubMed: 20920606]
27. Giansanti MG, Vanderleest TE, Jewett CE, Sechi S, Frappaolo A, Fabian L, Robinett CC, Brill JA, Loerke D, Fuller MT, Blankenship JT. Exocyst-Dependent Membrane Addition Is Required for Anaphase Cell Elongation and Cytokinesis in Drosophila. PLoS Genet. 2015;11(11):e1005632. Epub 2015/11/04. doi: 10.1371/journal.pgen.1005632. PubMed PMID: 26528720; PMCID: PMC4631508. [PubMed: 26528720]
28. Laks DR, Masterman-Smith M, Visnyei K, Angenieux B, Orozco NM, Foran I, Yong WH, Vinters HV, Liau LM, Lazareff JA, Mischel PS, Cloughesy TF, Horvath S, Kornblum HI. Neurosphere formation is an independent predictor of clinical outcome in malignant glioma. Stem Cells. 2009;27(4):980–7. Epub 2009/04/09. doi: 10.1002/stem.15. PubMed PMID: 19353526. [PubMed: 19353526]
29. Gao J, Aksoy BA, Dogrusoz U, Dresdner G, Gross B, Sumer SO, Sun Y, Jacobsen A, Sinha R, Larsson E, Cerami E, Sander C, Schultz N. Integrative analysis of complex cancer genomics and clinical profiles using the cBioPortal. Sci Signal. 2013;6(269):pl1. doi: 10.1126/scisignal.2004088. PubMed PMID: 23550210.
30. Cerami E, Gao J, Dogrusoz U, Gross BE, Sumer SO, Aksoy BA, Jacobsen A, Byrne CJ, Heuer ML, Larsson E, Antipin Y, Reva B, Goldberg AP, Sander C, Schultz N. The cBio cancer genomics portal: an open platform for exploring multidimensional cancer genomics data. Cancer Discov. 2012;2(5):401–4. Epub 2012/05/17. doi: 10.1158/2159-8290.CD-12-0095. PubMed PMID: 22588877; PMCID: PMC3956037. [PubMed: 22588877]
31. Kasza KE, Zallen JA. Dynamics and regulation of contractile actin-myosin networks in morphogenesis. Curr Opin Cell Biol. 2011;23(1):30–8. Epub 2010/12/07. doi: 10.1016/j.ceb.2010.10.014. PubMed PMID: 21130639; PMCID: PMC3320050. [PubMed: 21130639]
32. Cabernard C Cytokinesis in Drosophila melanogaster. Cytoskeleton (Hoboken). 2012;69(10):791–809. Epub 2012/08/14. doi: 10.1002/cm.21060. PubMed PMID: 22888045. [PubMed: 22888045]
33. Mitonaka T, Muramatsu Y, Sugiyama S, Mizuno T, Nishida Y. Essential roles of myosin phosphatase in the maintenance of epithelial cell integrity of Drosophila imaginal disc cells. Dev Biol. 2007;309(1):78–86. Epub 2007/07/31. doi: 10.1016/j.ydbio.2007.06.021. PubMed PMID: 17662709. [PubMed: 17662709]
34. Chougule AB, Hastert MC, Thomas JH. Drak Is Required for Actomyosin Organization During Drosophila Cellularization. G3 (Bethesda). 2016;6(4):819–28. Epub 2016/01/29. doi: 10.1534/g3.115.026401. PubMed PMID: 26818071; PMCID: PMC4825652. [PubMed: 26818071]
35. Gillespie GY, Soroceanu L, Manning TJ Jr., Gladson CL, Rosenfeld SS. Glioma migration can be blocked by nontoxic inhibitors of myosin II. Cancer Res. 1999;59(9):2076–82. Epub 1999/05/08. PubMed PMID: 10232591. [PubMed: 10232591]
36. Salhia B, Hwang JH, Smith CA, Nakada M, Rutka F, Symons M, Rutka JT. Role of myosin II activity and the regulation of myosin light chain phosphorylation in astrocytomas. Cell Motil Cytoskeleton. 2008;65(1):12–24. Epub 2007/09/27. doi: 10.1002/cm.20240. PubMed PMID: 17896341. [PubMed: 17896341]
37. Ivkovic S, Beadle C, Noticewala S, Massey SC, Swanson KR, Toro LN, Bresnick AR, Canoll P, Rosenfeld SS. Direct inhibition of myosin II effectively blocks glioma invasion in the presence of

multiple motogens. Mol Biol Cell. 2012;23(4):533–42. Epub 2012/01/06. doi: mbc.E11-01-0039 [pii] 10.1091/mbc.E11-01-0039. PubMed PMID: 22219380. [PubMed: 22219380]

38. Bornhauser BC, Olsson PA, Lindholm D. MSAP is a novel MIR-interacting protein that enhances neurite outgrowth and increases myosin regulatory light chain. J Biol Chem. 2003;278(37):35412–20. Epub 2003/06/27. doi: 10.1074/jbc.M306271200. PubMed PMID: 12826659. [PubMed: 12826659]
39. Beroukhim R, Getz G, Nghiemphu L, Barretina J, Hsueh T, Linhart D, Vivanco I, Lee JC, Huang JH, Alexander S, Du J, Kau T, Thomas RK, Shah K, Soto H, Perner S, Prensner J, Debiasi RM, Demichelis F, Hatton C, Rubin MA, Garraway LA, Nelson SF, Liau L, Mischel PS, Cloughesy TF, Meyerson M, Golub TA, Lander ES, Mellinghoff IK, Sellers WR. Assessing the significance of chromosomal aberrations in cancer: methodology and application to glioma. Proc Natl Acad Sci U S A. 2007;104(50):20007–12. Epub 2007/12/14. doi: 10.1073/pnas.0710052104. PubMed PMID: 18077431; PMCID: PMC2148413. [PubMed: 18077431]
40. Yan H, Parsons DW, Jin G, McLendon R, Rasheed BA, Yuan W, Kos I, Batinic-Haberle I, Jones S, Riggins GJ, Friedman H, Friedman A, Reardon D, Herndon J, Kinzler KW, Velculescu VE, Vogelstein B, Bigner DD. IDH1 and IDH2 mutations in gliomas. N Engl J Med. 2009;360(8):765–73. Epub 2009/02/21. doi: 10.1056/NEJMoa0808710. PubMed PMID: 19228619; PMCID: PMC2820383. [PubMed: 19228619]
41. Parsons DW, Jones S, Zhang X, Lin JC, Leary RJ, Angenendt P, Mankoo P, Carter H, Siu IM, Gallia GL, Olivi A, McLendon R, Rasheed BA, Keir S, Nikolskaya T, Nikolsky Y, Busam DA, Tekleab H, Diaz LA Jr., Hartigan J, Smith DR, Strausberg RL, Marie SK, Shinjo SM, Yan H, Riggins GJ, Bigner DD, Karchin R, Papadopoulos N, Parmigiani G, Vogelstein B, Velculescu VE, Kinzler KW. An integrated genomic analysis of human glioblastoma multiforme. Science. 2008;321(5897):1807–12. Epub 2008/09/06. doi: 1164382 [pii] 10.1126/science.1164382. PubMed PMID: 18772396. [PubMed: 18772396]
42. Guo C, Pirozzi CJ, Lopez GY, Yan H. Isocitrate dehydrogenase mutations in gliomas: mechanisms, biomarkers and therapeutic target. Curr Opin Neurol. 2011;24(6):648–52. Epub 2011/10/18. doi: 10.1097/WCO.0b013e32834cd415. PubMed PMID: 22002076; PMCID: PMC3640434. [PubMed: 22002076]
43. Jordan P, Karess R. Myosin light chain-activating phosphorylation sites are required for oogenesis in Drosophila. J Cell Biol. 1997;139(7):1805–19. Epub 1998/02/07. PubMed PMID: 9412474. [PubMed: 9412474]
44. Newell-Litwa KA, Horwitz R, Lamers ML. Non-muscle myosin II in disease: mechanisms and therapeutic opportunities. Disease models & mechanisms. 2015;8(12):1495–515. Epub 2015/11/07. doi: 10.1242/dmm.022103. PubMed PMID: 26542704; PMCID: PMC4728321. [PubMed: 26542704]
45. Beadle C, Assanah MC, Monzo P, Vallee R, Rosenfeld SS, Canoll P. The role of myosin II in glioma invasion of the brain. Mol Biol Cell. 2008;19(8):3357–68. Epub 2008/05/23. doi: E08-03-0319 [pii] 10.1091/mbc.E08-03-0319. PubMed PMID: 18495866. [PubMed: 18495866]
46. Wong SY, Ulrich TA, Deleyrolle LP, MacKay JL, Lin JM, Martuscello RT, Jundi MA, Reynolds BA, Kumar S. Constitutive activation of myosin-dependent contractility sensitizes glioma tumor-initiating cells to mechanical inputs and reduces tissue invasion. Cancer Res. 2015;75(6):1113–22. Epub 2015/01/31. doi: 10.1158/0008-5472.CAN-13-3426. PubMed PMID: 25634210; PMCID: PMC4359960. [PubMed: 25634210]
47. Field CM, Coughlin M, Doberstein S, Marty T, Sullivan W. Characterization of anillin mutants reveals essential roles in septin localization and plasma membrane integrity. Development. 2005;132(12):2849–60. Epub 2005/06/03. doi: 10.1242/dev.01843. PubMed PMID: 15930114. [PubMed: 15930114]
48. Field CM, Alberts BM. Anillin, a contractile ring protein that cycles from the nucleus to the cell cortex. J Cell Biol. 1995;131(1):165–78. Epub 1995/10/01. PubMed PMID: 7559773; PMCID: PMC2120607. [PubMed: 7559773]
49. Thomas JH, Wieschaus E. src64 and tec29 are required for microfilament contraction during Drosophila cellularization. Development. 2004;131(4):863–71. Epub 2004/01/23. doi: 10.1242/dev.00989. PubMed PMID: 14736750. [PubMed: 14736750]

50. Hickson GR, O'Farrell PH. Rho-dependent control of anillin behavior during cytokinesis. J Cell Biol. 2008;180(2):285–94. Epub 2008/01/23. doi: 10.1083/jcb.200709005. PubMed PMID: 18209105; PMCID: PMC2213597. [PubMed: 18209105]

SIGNIFICANCE

Findings reveal new insights into differential regulation of cell proliferation in malignant brain tumors, which will have a broader impact on research regarding mechanisms of oncogene cooperation and dependencies in cancer.

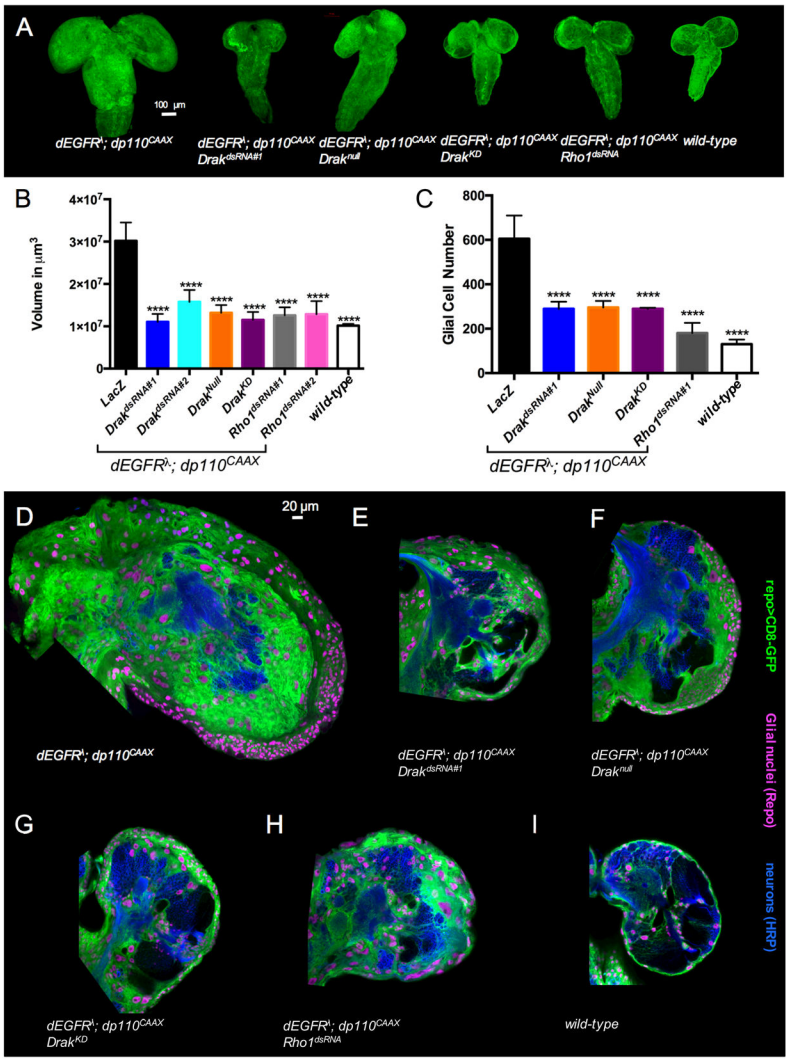

Figure 1. Drak is required for glial neoplasia in *Drosophila*.

(A) Optical projections of whole brain-nerve cord complexes from 3rd instar larvae approximately 130 hrs old. Dorsal view; anterior up. CD8-GFP (green) labels glial cell bodies. Knockdown of Drak (*repo>dEGFR$^{\lambda}$;dp110^{CAAX};Drak^{dsRNA}*) and Rho1 (*repo>dEGFR$^{\lambda}$;dp110^{CAAX};Rho1^{dsRNA}*), the Drak null genetic background (*Drak^{null}*; *repo>dEGFR$^{\lambda}$;dp110^{CAAX}*), or overexpression of catalytically inactive Drak (*repo>dEGFR$^{\lambda}$;dp110^{CAAX};Drak^{KD}*) decreased brain overgrowth relative to *repo>dEGFR$^{\lambda}$;dp110^{CAAX}*.

(B, C) (B) Total volumes (in μm^3) of 3rd instar larval brains, measured using Imaris. *repo>dEGFR$^{\lambda}$;dp110^{CAAX}*(n=3), *repo>dEGFR$^{\lambda}$;dp110^{CAAX};Drak$^{dsRNA\#1}$*(n=5), *repo>dEGFR$^{\lambda}$;dp110^{CAAX};Drak$^{dsRNA\#2}$*(n=5), *Drak^{null};repo>dEGFR$^{\lambda}$;dp110^{CAAX}*(n=3), *repo>dEGFR$^{\lambda}$;dp110^{CAAX};Drak^{KD}*(n=3), *repo>dEGFR$^{\lambda}$;dp110^{CAAX};Rho1$^{dsRNA\#1}$*(n=4), *repo>dEGFR$^{\lambda}$;dp110^{CAAX};Rho1$^{dsRNA\#2}$*(n=5), *wild-type*(n=3). (C) Glial cell numbers in representative 3 μm optical projections of 3rd instar brain hemispheres (n=3 per genotype). Statistics generated using One-Way ANOVA, ****p<0.0001.

(D-I) 3 μm optical projections of brain hemispheres, age-matched 3rd instar larvae. Frontal sections, midway through brains. Anterior up; midline to left. Repo (magenta) labels glial cell nuclei; CD8-GFP (green) labels glial cell bodies; anti-HRP (blue) counter-stains for neurons and neuropil. (D) *repo>dEGFR$^{\lambda}$;dp110^{CAAX}* showed increased glial cell numbers (magenta nuclei, green cell bodies) relative to (I) wild-type. (E-G) Drak knockdown (Drak^{dsRNA}), genetic reduction of Drak using a null allele (*Drak^{null}*), or overexpression of catalytically inactive Drak (*Drak^{KD}*) significantly reduced glial cells compared to *repo>dEGFR$^{\lambda}$;dp110^{CAAX}*.

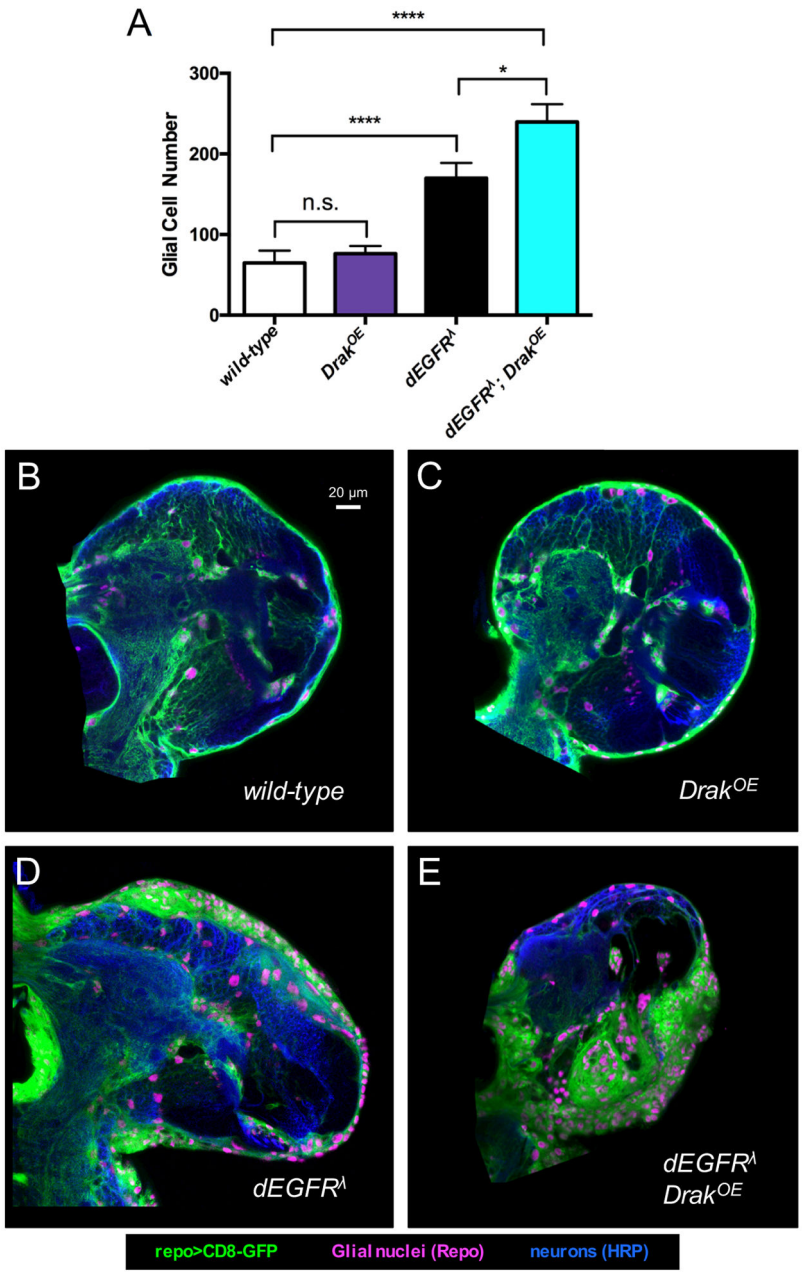

Figure 2. Drak cooperates with EGFR to promote glial transformation.

(A) Glial cell numbers in representative 3 µm optical projections of 3rd instar brain hemispheres. Statistics generated using One-Way ANOVA, ****p<0.0001. Comparisons of *wild-type* to $Drak^{OE}$ and $dEGFR^{\lambda}$ to $dEGFR^{\lambda};Drak^{OE}$ were performed using paired parametric T-Tests, n.s: p>0.05, *p<0.05. *wild-type*(n=5), $repo>Drak^{OE}$(n=7), $repo>dEGFR^{\lambda}$(n=4), $repo>Drak^{OE};dEGFR^{\lambda}$ (n=3).

(B-E) 3 µm optical projections of brain hemispheres from 3rd instar larvae, approximately 130 hrs old. Frontal sections, midway through brains. Repo (magenta) labels glial cell nuclei; CD8-GFP (green) labels glial cell bodies; anti-HRP (blue) counter-stains for neurons and neuropil. (A-B) Drak overexpression ($Drak^{OE}$) using *repo-Gal4* had no obvious effect

on glial cell development compared to wild-type. (A, C) *dEGFR*$^{\lambda}$ overexpression alone increased glial cells compared to wild-type. (D) *repo>dEGFR*$^{\lambda}$;*Drak*^{OE} showed increased numbers of abnormal glia (magenta nuclei, green cell bodies), compared to *Drak*^{OE} or *dEGFR*$^{\lambda}$ alone, which lost their normal stellate shape and formed aggregates that disrupt normal brain architecture and stunt brain development, evidenced by decreased neural tissue (HRP-stain).

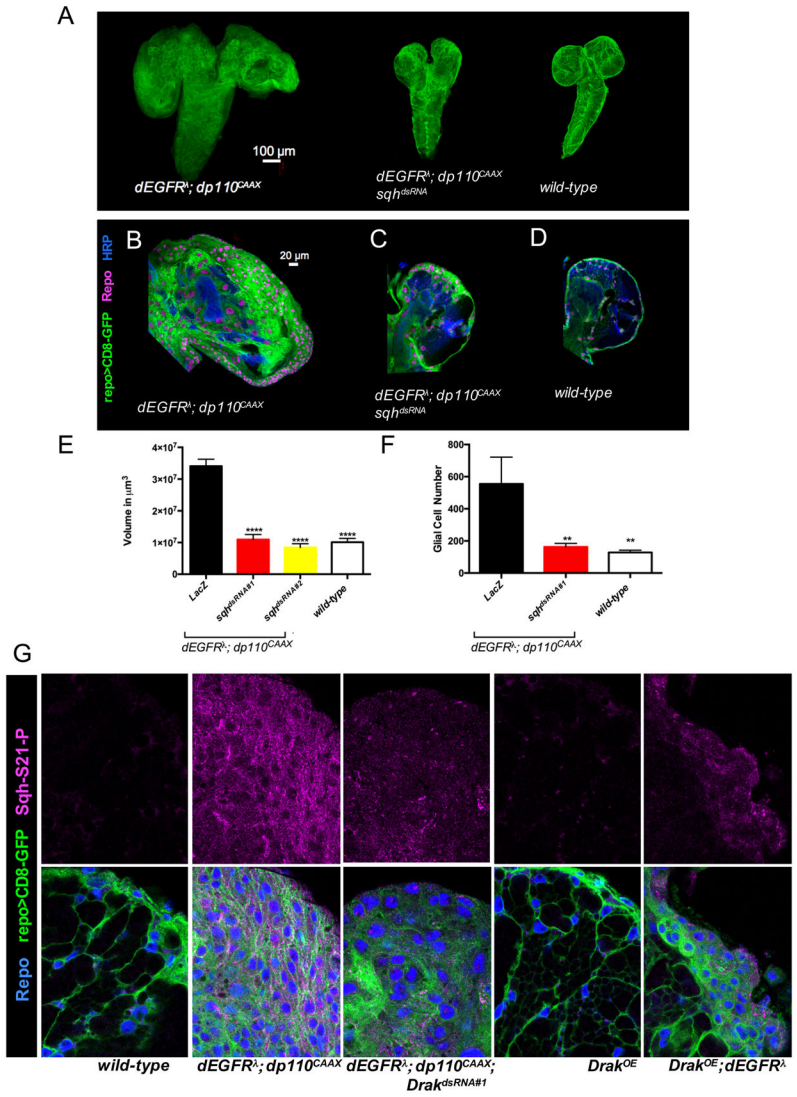

Figure 3. Drak acts downstream of oncogenic EGFR to phosphorylate Sqh.

(A) Optical projections of whole brain-nerve cord complexes from 3rd instar larvae approximately 130 hrs old. Dorsal view; anterior up. CD8-GFP (green) labels glia. Sqh knockdown (repo>dEGFRλ;dp110CAAX;sqhdsRNA) decreased neoplastic overgrowth relative to repo>dEGFRλ;dp110CAAX.

(B-D) 3 µm optical projections of brain hemispheres from age-matched 3rd instar larvae. Frontal sections, midway through brains. Repo (magenta) labels glial cell nuclei; CD8-GFP (green) labels glial cell bodies; anti-HRP (blue) counter-stains for neurons and neuropil. (B) repo>dEGFRλ;dp110CAAX showed increased glial cell numbers (magenta nuclei, green cell bodies) relative to (D) wild-type. (C) Drak knockdown dramatically reduced neoplastic glial proliferation compared to controls.

(E) Total volumes (in µm3) of 3rd instar larval brains, measured using Imaris. sqh RNAi in the context of dEGFRλ;dp110CAAX reduced brain volume compared to dEGFRλ;dp110CAAX controls. Statistics generated using One-Way ANOVA, **** $p<0.0001$. repo>dEGFRλ;dp110CAAX(n=3),

repo>dEGFRλ;dp110CAAX;sqhdsRNA#1(n=5),
repo>dEGFRλ;dp110CAAX;sqhdsRNA#2 (n=4), wild-type(n=3).
(F) Glial cell numbers in representative 3 μm optical projections of 3rd instar brain hemispheres. Statistics generated using One-Way ANOVA, **p<0.01 (n=3 per genotype).
(G) 3 μm optical projections of brain hemispheres from 3rd instar larvae. Repo (blue) labels glial cell nuclei; CD8-GFP (green) labels glial cell bodies; and Sqh-S21-P (magenta, Sqh-S21-P alone top panels, merge bottom panels). repo>dEGFRλ;dp110CAAX brains (second panel from left) showed increased Sqh-P21-P compared to wild-type (leftmost panel). Drak knockdown in dEGFRλ;dp110CAAX glia (middle panel) reduced Sqh-P21-P compared to repo>dEGFRλ;dp110CAAX glia (second panel from left). Co-overexpression of Drak and dEGFRλ increased Sqh-P21-P levels (rightmost panel) compared to Drak overexpression alone (second panel from right).

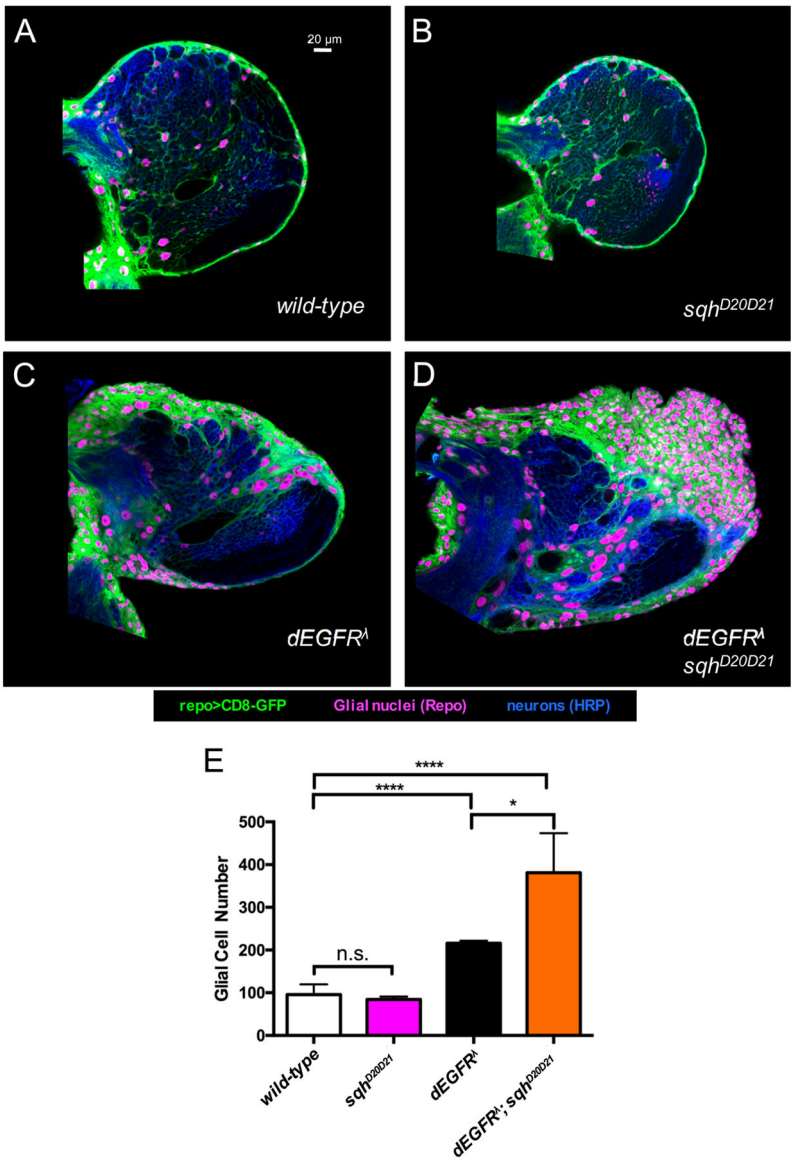

Figure 4. Sqh is a functionally relevant Drak substrate in glial neoplasia.

(A-D) 3 μm optical projections of brain hemispheres from 3rd instar larvae approximately 130 hrs old. Frontal sections, midway through brains. Repo (magenta) labels glial cell nuclei; CD8-GFP (green) labels glial cell bodies; anti-HRP (blue) counter-stains for neurons and neuropil. (B) *sqh*^{D20D21} overexpression in glia caused no observable phenotype compared to (A) wild-type. (D) *sqh*^{D20D21} and *dEGFR*$^{\lambda}$ co-overexpression yielded small proliferative glia that disturbed normal brain architecture, as compared to (A) wild-type and (C) *dEGFR*$^{\lambda}$ alone brains.

(E) Glial cell numbers in representative 3 μm optical projections of 3rd instar brain hemispheres. Statistics generated using One-Way ANOVA, ****p<0.0001; cell numbers of *wild-type* flies to *sqh*^{D20D21} flies compared using unpaired parametric T-Tests, n.s: p>0.05; *dEGFR*$^{\lambda}$ flies to *dEGFR*$^{\lambda}$*;sqh*^{D20D21} compared using paired parametric T-Tests, *p<0.05 (n=4 per genotype).

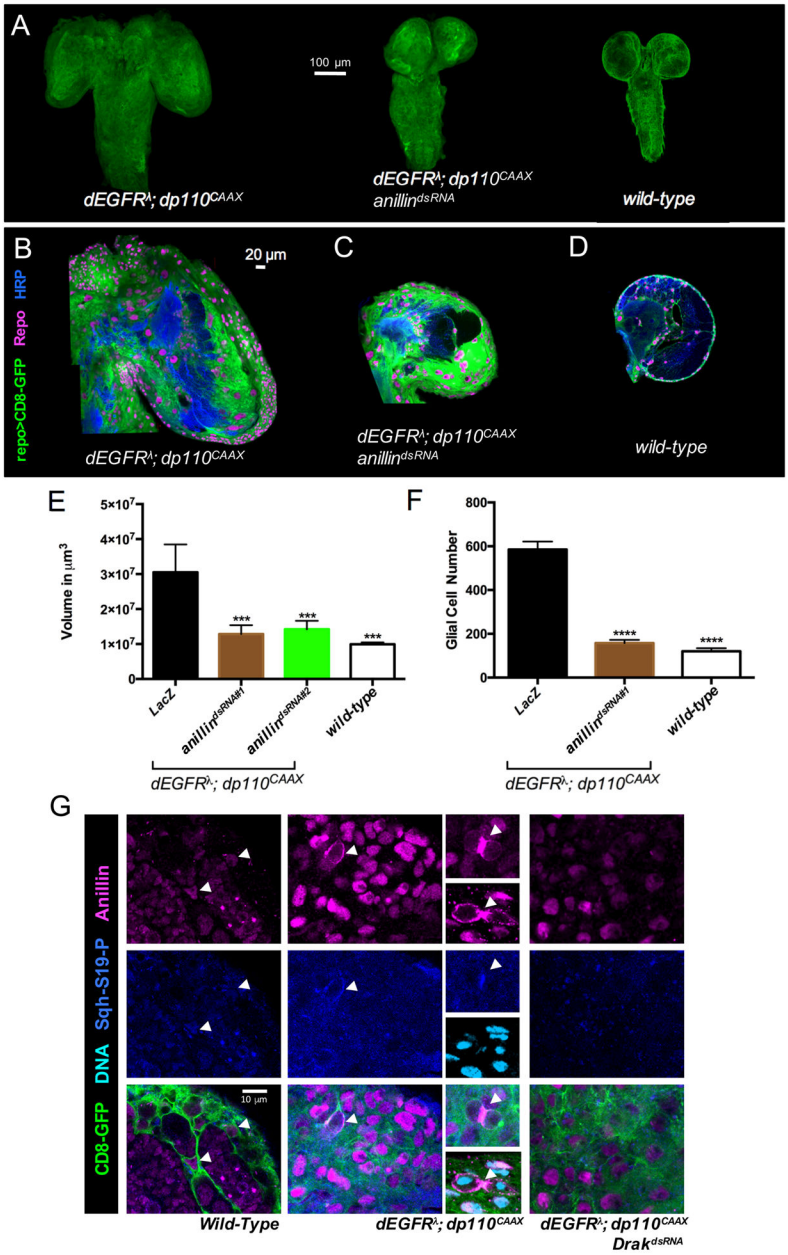

Figure 5. A Sqh binding partner, Anillin, is required for neoplastic growth.

(A) Optical projections of whole brain-nerve cord complexes from 3rd instar larvae approximately 130 hrs old. Dorsal view; anterior up. CD8-GFP labels glia (green). Knockdown of *anillin* (*repo>dEGFR$^{\lambda}$;dp110^{CAAX};anillin^{dsRNA}*) show decreased neoplastic brain overgrowth relative to *repo>dEGFR$^{\lambda}$;dp110^{CAAX}*.

(B-D) 3 μm optical projections of brain hemispheres from age-matched 3rd instar larvae. Frontal sections, midway through brains. Repo (magenta) labels glial cell nuclei; CD8-GFP (green) labels glial cell bodies; anti-HRP (blue) counter-stains for neurons and neuropil. (C) *anillin* knockdown dramatically reduced neoplastic glial proliferation in the context of *dEGFR$^{\lambda}$;dp110^{CAAX}* compared to *repo>dEGFR$^{\lambda}$;dp110^{CAAX}* controls (B).

(E) The total volume (in μm^3) of 3rd instar larval brains, measured using Imaris. *anillin* knockdown drastically reduced brain volume in the context of $dEGFR^{\lambda};dp110^{CAAX}$. Statistics generated using One-Way ANOVA, ***p<0.001. $repo>dEGFR^{\lambda};dp110^{CAAX}$ (n=3), $repo>dEGFR^{\lambda};dp110^{CAAX};anillin^{dsRNA\#1}$(n=4), $repo>dEGFR^{\lambda};dp110^{CAAX};anillin^{dsRNA\#2}$(n=4), *wild-type*(n=3).

(F) Glial cell numbers in representative 3 μm optical projections of brain hemispheres from 3rd instar larvae. Statistics generated using One-Way ANOVA with multiple comparisons, ****p<0.0001 (n=3 per genotype).

(G) 3 μm optical projections, 3rd instar larval brains. CD8-GFP (green) labels glial cell membranes. (F) immunostaining showed low levels of Anillin protein (magenta, upper panel) and Sqh-S21-P (blue, middle panel) in glia (white arrows, green, lower panel) and neighboring neurons (GFP-negative) in wild-type. (G) high levels of Anillin protein (magenta, upper panels) and Sqh-S21-P (blue, middle panel) were detected in $dEGFR^{\lambda};dp110^{CAAX}$ neoplastic glia (lower panel), with Anillin showing nuclear localization and Sqh-S21-P showing cytoplasmic localization in non-mitotic cells. In mitotic cells (white arrow, in large panel), Anillin and Sqh-S21-P showed membrane and cytoplasmic co-localization. In cytokinesis, Anillin localized to the cleavage furrow (white arrows in insets), with upper inset showing cells in cytokinesis co-stained with Anillin and Sqh-S21-P with the lower inset showing cells in cytokinesis co-stained Anillin and DRAQ7 DNA dye (cyan) to show cell nuclei. (H) immunostaining revealed reduced levels of Anillin protein (magenta, upper panel) and Sqh-S21-P (blue, middle panel) upon *Drak* RNAi in $dEGFR^{\lambda};dp110^{CAAX}$ glia.

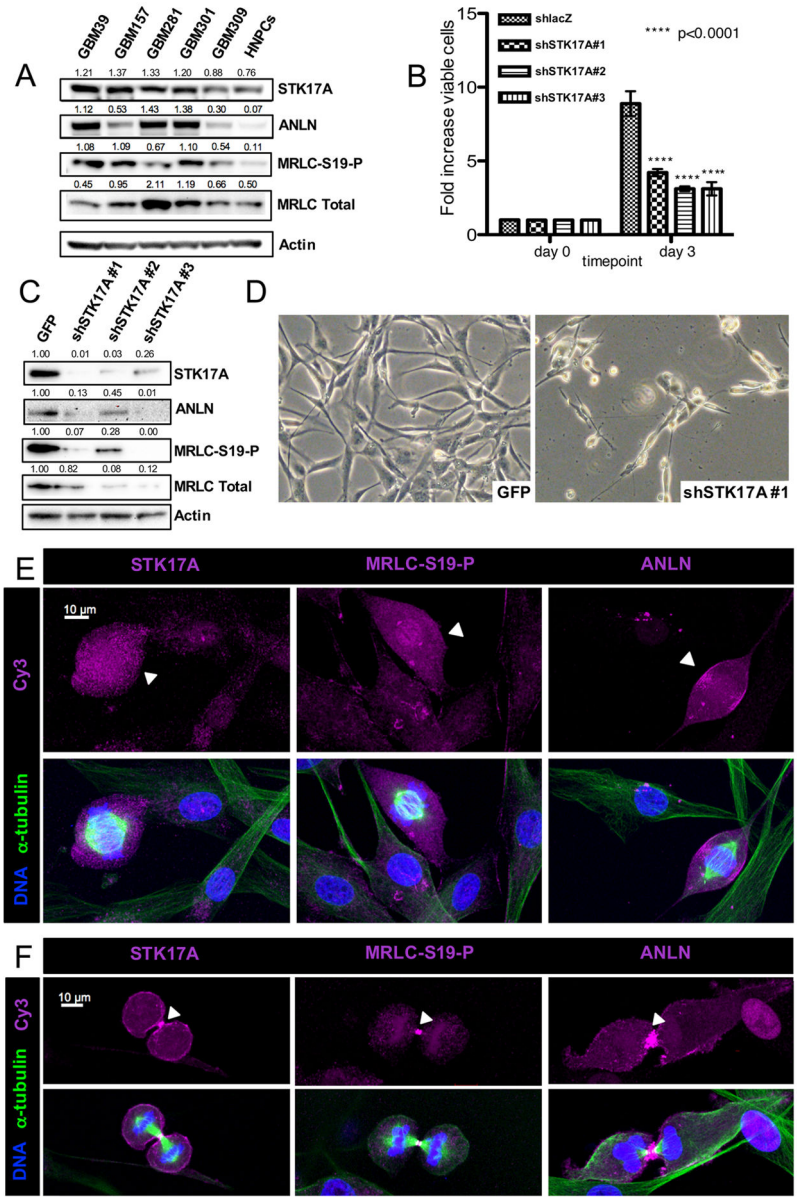

Figure 6. STK17A function is required for GBM cell proliferation, and regulates MRLC phosphorylation and ANLN expression.

(A) Panel of GBM gliomasphere cultures. GBM39 and GBM301 harbor amplified $EGFR^{VIII}$; GBM281 harbors an activated variant mutant EGFR; GBM157 is PDGFR-overexpressing; GBM309 has neither (15, 28). Band intensities were normalized to Actin (numbers above bands).

(B) WST-1 Assay on U87 cells. Following selection for shRNA expression, U87 cell proliferation was measured by WST-1 reagent and quantified as fold-increase in absorbance between day 0 and day 3 after plating, normalized to controls treated with nontargeting shRNA. 3 shRNAs tested for STK17A. p-values from One-Way ANOVA with Dunnett post-test.

(C) STK17A knockdown using 3 separate shRNAs in GBM301 decreased expression of ANLN and MRLC-S19-P compared to control cells treated with GFP shRNAs; all samples treated with ZVAD (Supplemental Figure S4C-D shows non-ZVAD treated cells). Cells were infected with lentiviral vectors 3 days prior to harvest. Band intensities were normalized to Actin (numbers above bands), reported as fold changes relative to control cells.
(D) Adherently cultured GBM301 cells 3 days after infection with control lentivirus or shSTK17A#1, which reduced proliferation and altered cell shape and reduced adhesion; cells treated with ZVAD for 24 hrs prior to imaging.
(E, F) U87-EGFR^{VIII} cells were fixed and probed for either STK17A, phosphorylated MRLC (MRLC-S19-P), or ANLN (magenta) and α-tubulin (green) and DRAQ7 to label DNA (blue). (E) STK17A, MRLC-S19-P, and ANLN were upregulated in tumor cells undergoing mitosis (cells marked with white arrows). (F) STK17A, MRLC-S19-P, and ANLN were localized in the cleavage furrow of tumor cells undergoing cytokinesis (cells marked with white arrows).

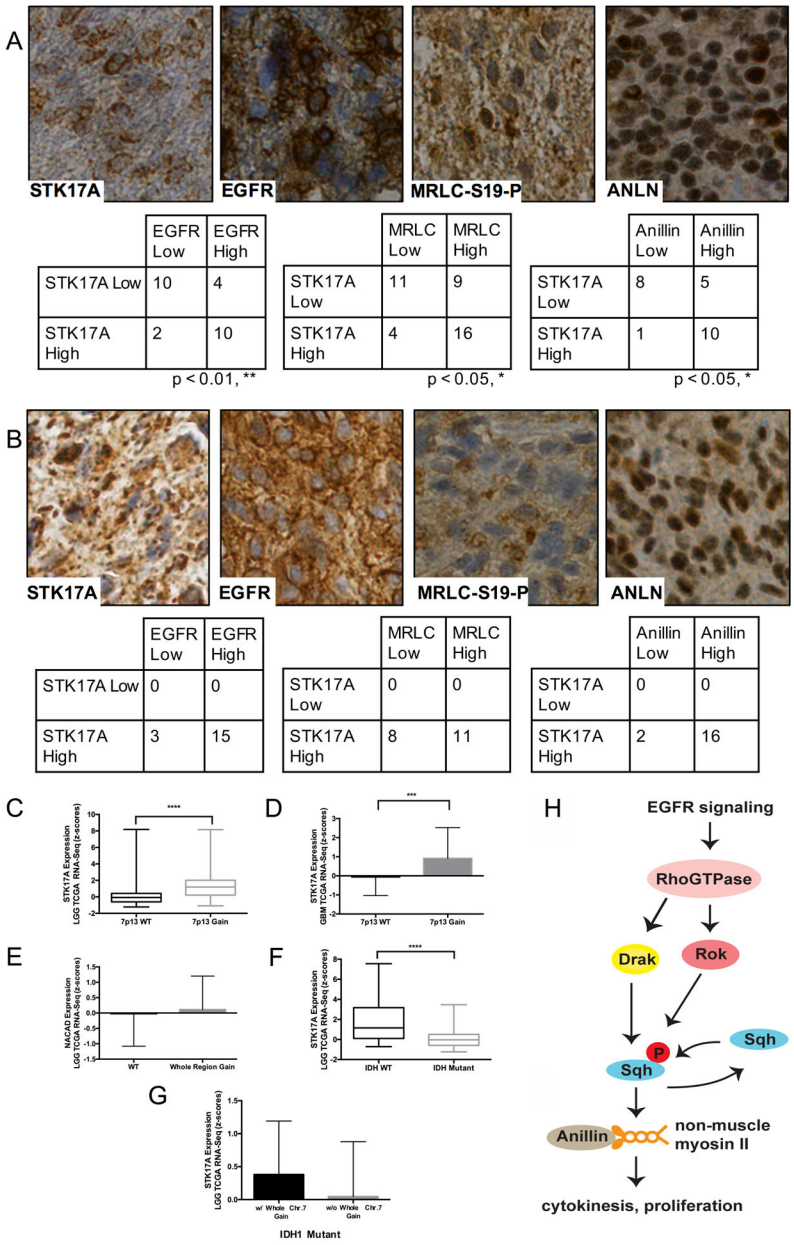

Figure 7. STK17A expression correlates with EGFR status, MRLC-S19-P levels, and ANLN expression in human tumors.

(A, B) Immunohistochemistry on TMAs of human (A) LGG tissue or (B) GBM tissue for STK17A, EGFR, MRLC-S19-P, or ANLN (reddish brown) showing cytoplasmic enrichment in tumor cells. Hematoxilin counterstain. Statistical analysis of low grade glioma of (A) LGG tumor specimens expressing STK17A show a statistically significant (Fisher's Exact Test) correlation between high STK17A expression and high EGFR expression, high MRLC-S19-P expression, and high ANLN expression. (B, lower) Table of the number of GBM tumor specimens with either high or low expression of STK17A and high or low expression of either EGFR, MRLC-S19-P, or ANLN.

(C-G) Analysis of *STK17A* mRNA expression in relation to chromosome 7 gain, NACAD expression, and IDH1 status in LGGs and GBMs using TCGA datasets. Statistics generated using Mann-Whitney *U* test, ****p<0.0001, ***p<0.001 (number of TCGA cases used: C:282, D:160, E:281, F:250, G:219).

(H) Diagram depicting the role of Drak/STK17A in promoting gliomas.